Geophys. J. Int. (2006) **164,** 182–191 doi: 10.1111/j.1365-246X.2005.02804.x

CGPS time-series and trajectories of crustal motion along the West Hellenic Arc

Ch. Hollenstein,[1] A. Geiger,[1] H.-G. Kahle[1] and G. Veis[2]

[1]*Geodesy and Geodynamics Lab, Institute of Geodesy and Photogrammetry, ETH Zürich,* CH-8093 *Zürich, Switzerland. E-mail: hollenst@geod.baug.ethz.ch*
[2]*Higher Geodesy Lab, NTU Athens, Greece*

Accepted 2005 September 19. Received 2005 August 25; in original form 2005 February 17

SUMMARY

Western Greece is one of the seismotectonically most active regions in Europe. The main tectonic structures are the West Hellenic Arc (WHA) and the Kephalonia Fault Zone. In order to monitor and understand the crustal movements in space and time, a continuous GPS network was installed. In this paper we present results of 6 yr (1995–2001) of measurements. To ensure a consistent reference frame, 54 mainly European IGS and EUREF sites were included in the processing. A selected subset was used to estimate an Euler pole for the rotation of Eurasia. In order to obtain coordinate time-series of high precision that are representative for crustal deformation, special emphasis was given to the elimination of non-tectonic effects. Four steps of improvement were pursued, including a reprocessing after exclusion of poor data, the removal of remaining outliers, the correction of unknown phase centre offsets after antenna changes and weighted common-mode filtering. With this procedure, non-tectonic irregularities were reduced significantly, and the precision was improved by an average of 40 per cent. The final time-series are used as a base for depicting trajectories of crustal motion, interpreting the temporal behaviour of the sites and for estimating velocities. For the first time, height changes in the WHA area were detected and quantified by GPS. Sites that are located near the epicentres of the 1997 Strofades ($Mw = 6.6$) and the 1999 Athens ($Mw = 6.0$) earthquakes are particularly considered.

Key words: fault motion, geodynamics, GPS, Greece, seismotectonics, West Hellenic Arc.

1 INTRODUCTION

The area of the Ionian islands, western Greece, is associated with a distinct kinematic field of recent crustal movements in the collision zone between the African and Eurasian lithospheric plates. Numerous earthquakes confirm the high seismotectonic activity. Main tectonic features are the West Hellenic Arc (WHA), where the African plate is subducted under the Aegean microplate, and the Kephalonia Fault Zone (KFZ), a prominent dextral strike-slip fault, which terminates the WHA in the northwest (Fig. 1). Previous GPS results allowed to distinguish between two main kinematic fields separated by the KFZ. To the northwest of the KFZ, the motion is similar to the Eurasian one, while to the southeast of the KFZ, a southwestward motion with rates of up to more than 30 mm yr^{-1} was observed (Kahle *et al.* 1995; Cocard *et al.* 1999; Peter 2001). In order to obtain more detailed information about the crustal motion in this area, especially about the temporal variation in connection with the occurrence of earthquakes, a continuous GPS network was installed. We evaluated the data for the time period 1995–2001 to produce coordinate time-series. To realize a Eurasia-fixed reference frame, 54 IGS and EUREF stations were included in the processing and an Euler pole of rotation was calculated for Eurasia. To obtain reliable tectonic signals, non-tectonic effects were mitigated as much as possible. Therefore, an emphasis is placed on the improvement of the time-series. We document the different steps and discuss their influences on the results, which could be significantly improved. We present the final time-series, which are also visualized in terms of trajectories of crustal motion and used to calculate velocities. Special attention is given to the vertical components and to the Strofades (1997, $Mw = 6.6$) and the Athens (1999, $Mw = 6.0$) earthquakes, which both occurred near GPS sites.

2 GPS NETWORKS AND EVALUATION

The installation of a continuous GPS network was commenced in the Ionian Sea in 1995 (Peter *et al.* 1998; Peter 2001) and since then successively extended. To ensure a consistent reference frame, the data of 54 stations of the global IGS and the European EUREF networks (IGS: International GPS Service, http://igscb.jpl.nasa.gov; EUREF: European Reference Frame, http://www.euref-iag.org) were evaluated together with those from the Greek network. Their locations are shown in Fig. 1.

The data were processed on a daily basis using the Processing Engine (BPE) of the Bernese GPS software 4.2 (Beutler *et al.*

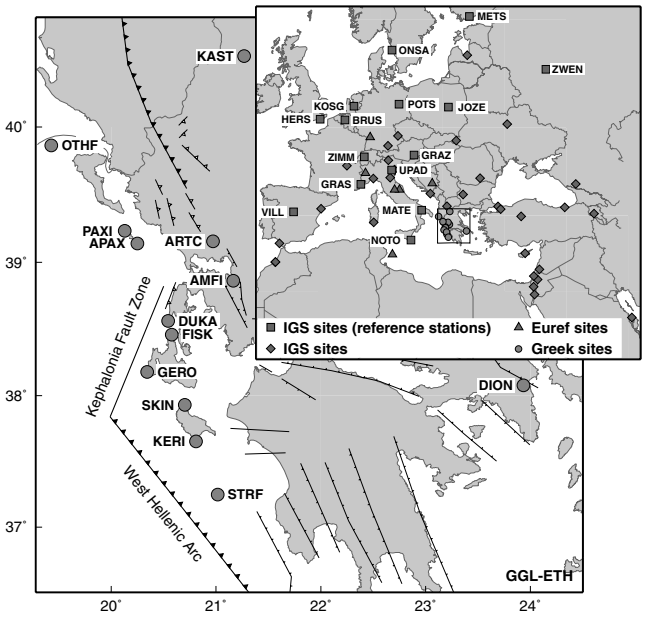

Figure 1. GPS network: location of GPS stations that have been processed in common.

2001), which uses a double-difference processing strategy. We used IGS precise orbits and the corresponding earth rotation parameters. If necessary, they were transformed using the program trnfsp3n (Kouba 2002) in order to keep all these data (as well as the site coordinates) in the same ITRF system. The baselines/single-difference phase files were constructed based on a maximum observations strategy. The ambiguities were resolved using the 'quasi-ionosphere-free' (QIF) strategy or the 'SIGMA'-strategy (when L2-squaring type receivers were present). Only observations above an elevation cut-off angle of 10° were used in the parameter estimation, and an elevation-dependent weighting was applied. We estimated one troposphere parameter per hour and station, and we used the Dry–Niell mapping function (Niell 1996). The whole network was processed taking into consideration the full variance–covariance information. As a result, daily solutions with daily coordinates were obtained, only weakly constrained to the reference frame. In order to maintain the good inner precision of the network, it was not fixed to reference points, but transformed using a Helmert transformation. 15 carefully selected European IGS stations (see Fig. 1) with their official ITRF coordinates and velocities were chosen as reference stations. For each day, an individual set of seven Helmert parameters was estimated to transform the network onto the reference stations. ITRF2000 (Altamimi *et al.* 2002) was used as reference frame.

3 EULER POLE FOR THE ROTATION OF EURASIA

In order to produce time-series and velocities in a consistent Eurasia-fixed frame, we first estimated an Euler pole for the motion of the Eurasian plate relative to ITRF2000. Several iterations of a least-squares adjustment were carried out using the final ITRF2000 velocities of the processed IGS and EUREF sites. Stations that obviously do not move like Eurasia (such as sites in Africa, Arabia, Israel or Turkey) were excluded from the beginning; also sites with time-series shorter than 2 yr were not included. After each iteration, the standardized velocity residuals of all included sites were

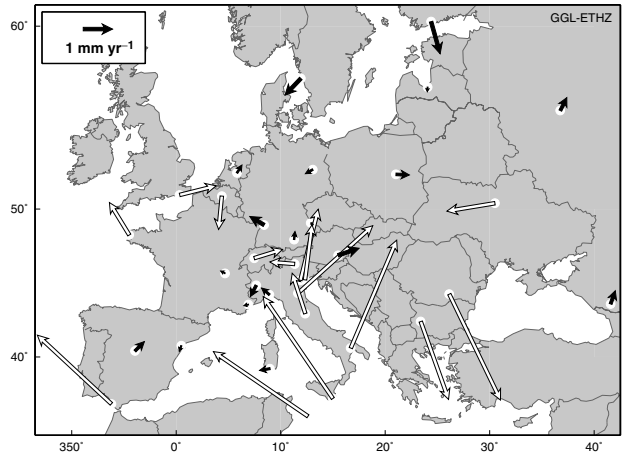

Figure 2. Velocity residuals with reference to the rotation of Eurasia (rotation parameters see chapter 3). Black arrows: velocities of sites which were included in the final pole estimation, white arrows: velocities of sites that were excluded during the iterations.

statistically tested using a *t*-test at the significance level of 5 per cent. Sites that did not pass the test were excluded. After eight iterations, all the 19 remaining sites (of initially 35) passed the test. The residuals of their geocentric velocity components are smaller than 0.75 mm yr^{-1}. The resulting pole is located at $56.3 \pm 0.7°$N/$101.0 \pm 1.1°$W, and the rotation rate is $0.254 \pm 0.002°$ Myr^{-1}.

This pole differs slightly from the pole determined by Altamimi *et al.* (2002); by 1.7° and 1.6° in southern and western direction, respectively, and by 0.006° Myr^{-1} in the rotation rate, corresponding to velocity differences of less than 0.5 mm yr^{-1} for Europe. The difference between the two pole solutions, which is within the margin of error (95 per cent) given by Altamimi *et al.* (2002), is mainly caused by the selection of the sites, which presumably represent the motion of Eurasia and which are used in the estimation of the rotation pole. Our strategy of iterative estimation, statistical testing and site exclusion yielded a different site selection.

The velocity residuals with respect to the rotation of Eurasia calculated above (=Eurasia-fixed velocities) of the sites that were included in the iteration process are shown in Fig. 2. It is seen that the sites whose velocities contributed to the estimation of the pole are well distributed over Europe, reaching from Spain and Italy across Central Europe to Scandinavia and Russia. The horizontal velocity residuals of these sites are all smaller than 0.8 mm yr^{-1}, with the exception of METS, which shows 1.1 mm yr^{-1}. Among the excluded sites, we clearly recognize the areas with non-Eurasian velocity fields: southern Spain and Italy, which show Africa-like movements; southeastern Italy, which moves northeastwards; and the sites in Bulgaria and Romania, which are south–southeast directed in their motion.

4 TIME-SERIES AND THEIR IMPROVEMENT

To obtain topocentric time-series relative to Eurasia, the geocentric coordinates were first transformed to topocentric coordinates. Then, we subtracted the part of the rotation of Eurasia, calculated as theoretical site velocities using the rotation parameters given above.

Because the time-series contain outliers, offsets and irregularities, which are not of tectonic origin, we used the following strategy to reduce them and to improve the precision:

(1) exclusion of poor data and complete reprocessing,

(2) elimination of remaining outliers,
(3) estimation and correction of antenna change offsets and
(4) weighted common-mode filtering.

Fig. 3 shows, for example, the time-series of the site KERI in its initial form ('KERI run 1 raw') and after having applied different steps of improvement. The arrows indicate irregularities that are eliminated by the subsequent step of improvement. Velocities and coordinate weighted root mean square (WRMS) errors were calculated by means of a weighted linear regression. The formal errors of the velocities (calculated under white noise conditions) were scaled by a factor of 4 in order to account for time-correlated noise. This mean scale factor is based on autocorrelation analyses of the time-series of the Greek network (Heller 2004). It is in concordance with scale factors found in previous studies (see e.g. Zhang *et al.* 1997; Mao *et al.* 1999; Caporali 2003).

4.1 Exclusion of poor data and complete reprocessing

The reason for most of the major irregularities in the time-series is the contribution of stations with data of poor quality. A poor station—especially, if it is a reference station—can significantly

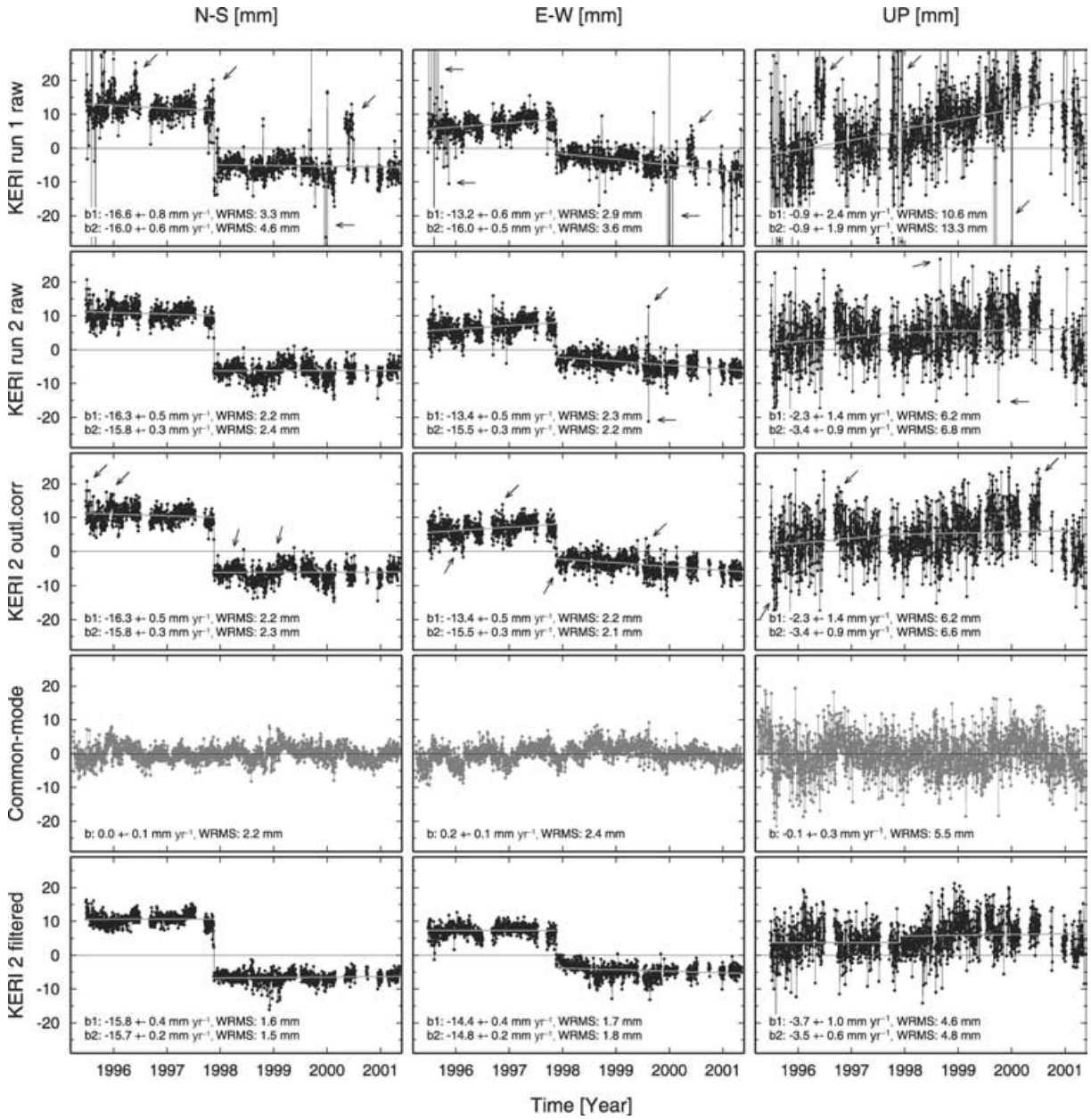

Figure 3. Detrended time-series for the station KERI, showing the improvement by excluding poor data, removing outliers and introducing a weighted common-mode filter. KERI run 1 raw: initial time-series resulting from the first processing run. KERI run 2 raw: resulting from the second processing run with exclusion of poor data (improvement step 1). KERI 2 outl.corr: after removal of remaining outliers (step 2). Common-mode: weighted common-mode signal (of nine sites in Greece). KERI 2 filtered: after weighted common-mode filtering (step 4). The offset in 1997, visible in all of the KERI-plots, is a co-seismic displacement caused by the $Mw6.6$ Strofades earthquake. 'b': velocity relative to Eurasia, calculated by weighted linear regression before detrending, formal error scaled by 4 (see chapter 4); b1: before, b2: after the earthquake. 'WRMS': weighted rms of daily coordinates. The grey straight lines represent the weighted linear fit. The arrows indicate irregularities that are eliminated by the subsequent step of improvement.

influence the whole network or part of it. For each day, the results and quality parameters of the GPS processing were screened to detect poor stations, which consequently were excluded for that particular day. The main criteria for exclusion were defined for: percentage of poor code data (>50 per cent), rms of code single point solution (>40–150 m), rms of triple-difference solution (>15–25 mm), percentage of resolved ambiguities (<60–30 per cent for QIF strategy), and coordinate rms (formal error >3–4 mm for horizontal or >5–8 mm for vertical coordinates). Additional criteria were: too few data, too many cycle slips, ambiguities or large residuals, too large rms after ambiguity resolution, outliers of coordinate values and external quality information (such as IGSMAIL or EUREFMAIL). For the reference stations, we used more rigorous criteria (first number in the ranges above) than for non-reference stations. During the evaluated time span of 2230 days (1995–2001), 73 stations measured totally 84 018 station days. 2200 of them were excluded. This corresponds to 2.6 per cent, or an average of about 10 days per station per year, or every day 1 station.

Afterwards, a complete reprocessing of the GPS measurements without the poor station days was carried out. The results show a significant improvement: most irregularities and outliers disappeared from the time-series, and the precision—represented by the velocity precision and the WRMS of a weighted linear fit—was improved by an average of 25 per cent. The vertical components of the velocity results and, for a few sites with only few data in the time span of evaluation, also the horizontal components of the velocity results changed by several mm yr^{-1}.

As an example, the improvement for the station KERI is shown in Fig. 3 ('KERI run 2 raw'). The fact that so many irregularities have disappeared and that the precision was improved by 10–20 per cent (horizontal)/50 per cent (vertical), although only 3 days of KERI data were excluded, means that almost all irregularities arose from other stations. This proves that poor data of a station have a considerable influence on the coordinate solutions of other stations. With this improvement (step 1), we eliminate the poor data only at the causing stations and can avoid removing all the corresponding daily coordinates of influenced stations in step 2 (chapter 4.2). The offset in 1997, still visible in the plot after step 1 (Fig. 3), is a coseismic displacement caused by the $Mw6.6$ Strofades earthquake on 1997 November 18.

4.2 Elimination of remaining outliers

In step 2, remaining outliers were removed from the time-series. Following Wdowinski *et al.* (1997), we defined as outliers: (a) daily coordinates with formal error (from GPS evaluation) larger than three times the mean formal error of the site and/or (b) coordinates that differ by more than three times the WRMS from a regression line. For time-series with an offset, separate linear trends for the two parts were calculated; and for time-series with large oscillations, higher degree regression was used instead of linear regression. The removal of remaining outliers from the time-series led to a further improvement of precision of about 5 per cent (WRMS as well as σ of velocities).

4.3 Estimation and correction of antenna change offsets

Apparent discontinuous position changes (in the time-series), which can be assigned to unknown variations of phase centre offsets due to an antenna change (in the following called 'antenna change offsets') were estimated and corrected. We calculated the antenna change

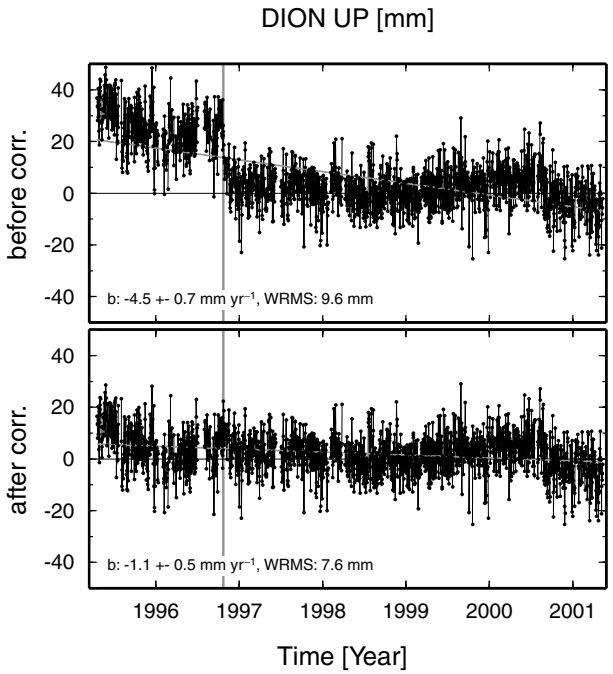

Figure 4. Correction of unknown variation of the phase centre offset due to an antenna change for the up-component of DION. Time-series before and after the correction (step 3). The vertical grey line marks the time of the antenna change. 'b': velocity, calculated by weighted linear regression, formal error scaled by 4 (see chapter 4); 'WRMS': weighted rms of daily coordinates.

offsets dx for each component using

$$dx = \overline{x}_2 - \overline{x}_1 - b \cdot (\overline{t}_2 - \overline{t}_1) \quad (1)$$

where b is the slope, calculated by weighted linear regression over the largest possible time span, which does not extend beyond the antenna change offset and other major irregularities. The indices 1 and 2 indicate time windows before and after the offset, respectively. Appropriate window lengths between several weeks and months were chosen according to the properties of the particular time-series. In our case, they were not extended over data gaps longer than 2 weeks and offsets or oscillations larger than two times the WRMS. $\overline{x}$ is the weighted coordinate average and $\overline{t}$ the mean time of the indicated window. For the sites in Greece, such a correction of an antenna change offset was applied to the time-series of DION (Fig. 4).

4.4 Weighted common-mode filtering

The final step of improvement is a common-mode filtering (Wdowinski *et al.* 1997). It is thereby assumed that signals common to all sites, which are located on different lithospheric blocks (which is the case for the sites in Greece), are most likely not of tectonic origin. Such signals can be filtered out of the time-series without loosing tectonic signals. Compared to Wdowinski *et al.* (1997), we expanded the standard common-mode filtering to a weighted common-mode filtering (Hollenstein 2000; Peter 2001) in order to handle data of variable quality. The algorithm consists of the following steps (each component is treated separately):

(1) **Detrending**: Removal of the main trend by weighted linear regression. The results are daily residuals for each site.

(2) **Stacking**: Calculation of the daily common-mode residuals using a weighted average.

$$\overline{r}(t) = \frac{\sum_{s=1}^{S}(p_s(t) \cdot r_s(t))}{\sum_{s=1}^{S} p_s(t)} \quad (2)$$

where $\overline{r}(t)$ is the weighted average residual (common-mode) for day t, S the number of sites included in the stacking procedure, $r_s(t)$ the residual for site s on day t, and $p_s(t)$ the weight of $r_s(t)$ computed as $p_s(t) = \frac{1}{(a_s \cdot \sigma_s(t))^2}$ with $\sigma_s(t)$ equal to the coordinate rms of day t and a_s as additional quality factor.

(3) **Filtering**: Removal of the corresponding common-mode residuals from the daily coordinates of each site.

We filtered only the sites in Greece, because the filter is more effective for this regional area. For the stacking, only stations without exceptional behaviour (like pre-, co- or post-seismic effects or large oscillations) should be considered. In our case, we used nine Greek sites; four with normal weight ($a_s = 1$, for long and quite complete time-series) and five with lower weight ($a_s = 2$, for shorter or often interrupted time-series). The filter was then applied to all the sites in Greece. The common-mode signals of the three components are shown in Fig. 3. They are significantly different from white noise. An annual oscillation (especially in the east component) and other signals are clearly visible. Many of them are also seen in the unfiltered time-series of KERI (arrows in Fig. 3, 'Keri 2 outl.corr') and have disappeared in the filtered time-series. Besides the removal of irregularities, the filter also reduced the scatter of daily coordinates. However, the co-seismic displacement in 1997 (as a tectonic signal) remained.

The application of the weighted common-mode filter improved the precision by about 20 per cent, and also changed the results for some velocities. The total improvement of precision (standard deviation of velocities and WRMS) between the first results (processing run 1) and the filtered time-series (after step 4) averaged at 40 per cent; some stations even showed an improvement of up to 80 per cent. We reached an average WRMS of about 2 mm for horizontal and 6 mm for vertical daily coordinates.

5 RESULTS AND DISCUSSION

Fig. 5 shows the time-series of the filtered daily coordinates (relative to Eurasia) for all sites in Greece. In addition, the crustal motion and its spatial distribution is visualized by means of trajectories. The trajectories displayed in Fig. 6 were produced from common-mode filtered time-series, which, in addition, were slightly smoothed by a Gaussian filter with a window size of 7 days. Table 1 summarizes the velocities and coordinate WRMS derived from the filtered time-series. The velocities are also plotted as insets in Fig. 6.

In general, the results for the horizontal velocity components confirm findings of previous studies (Cocard *et al.* 1999) and help to refine parts of them. The new reference frame ITRF2000 (instead of ITRF96), its realization by Helmert transformation on up to 15 IGS sites (instead of fixing on few sites) and the new pole of rotation of Eurasia yield self-consistent results. One refinement is that the rates in northern Greece are significantly different from the motion of Eurasia. KAST moves southwards with 3.1 ± 0.1 mm yr^{-1}. The velocities of the IGS sites in Bulgaria and Romania suggest that this non-Eurasian southward movement is already encountered farther north (see Fig. 2). We can confirm the opposite direction of motion to the northwest and to the southeast of the KFZ, which is consistent with the dextral sense of this strike-slip fault. To the northwest of the KFZ, we obtain a northward movement of 1.9 ± 0.2 mm yr^{-1} (APAX) and 2.9 ± 0.3 mm yr^{-1} (PAXI), respectively. The island of Othoni (OTHF) is moving towards west–northwest at a rate of 3.3 ± 0.6 mm yr^{-1}. To the southeast of the KFZ, the southwestward motion successively increases from 7 mm yr^{-1} up to more than 30 mm yr^{-1} within a north–south distance of less than 200 km. Another prominent feature is the large extensional deformation on the island of Zakinthos, which is clearly visible in the trajectories of crustal motion (Fig. 6). The lengthening of the baseline between northern (SKIN) and southern (KERI) Zakinthos is 6 mm yr^{-1}, corresponding to a strain rate of 190 nstrain yr^{-1}. A conspicuous cluster of microseismic events has occurred in the recent past in the vicinity of Zakinthos, which can be associated with the anomalous crustal deformation observed. The ongoing large baseline lengthening on this island indicates that this area is a high earthquake prone region.

Apart from linear movements, the high-resolution temporal behaviour of crustal deformation can be derived from the time-series. This was impossible on the basis of campaign measurements alone. While there is high seismic activity in the WHA area, in general, most time-series and trajectories are surprisingly linear; see for example KAST, DUKA, GERO and DION. In contrast, PAXI has quite a strange behaviour, which is not found at any other station of the network. A distinct linear oscillation, present in all the three components, with a period of 1 yr and an amplitude of 15 mm is clearly visible. The cause for this periodic behaviour is still unknown. We favour a local origin, because even the neighbouring station APAX, which is only 15 km away, does not show such a behaviour. The oscillation of PAXI is superimposed on a linear trend of motion of the same order of magnitude as the one for APAX. If only a small number of campaign measurements were available, a wrong model of a linear motion could lead to significant deviations of the velocity solution, depending on the times when the campaigns were conducted.

The most striking effects in the time-series and trajectories are the co-seismic slips at KERI and STRF caused by the $Mw6.6$ Strofades earthquake on 1997 November 18. On the basis of campaign measurements, Cocard *et al.* (1999) found seismically induced displacements of 120 mm towards south for STRF and 15 mm towards the southwest for KERI. We obtained an equal co-seismic displacement for STRF (south component: 117 ± 2 mm, east component: 12 ± 2 mm) and a slightly larger one for KERI (south component: 17 ± 1 mm, west component: 11 ± 1 mm). In addition, a co-seismic uplift was detected at the two sites: 90 ± 4 mm at STRF and 2 ± 2 mm at KERI. The uplift of STRF is also confirmed by our tide gauge measurements (Fig. 7). We furthermore compared the displacements of the GPS-sites with the location and fault plane solution of the earthquake (Fig. 6). It was a shallow thrusting event with a small strike-slip component and was attributed to the overthrusting of the Hellenic nappes over the subducting African plate. The co-seismic uplift is consistent with this mechanism and the upper plate structure along the WHA (proposed by Laigle *et al.* 2004). The horizontal displacements, especially the large south component at STRF, cannot be explained by this single fault plane solution shown in Fig. 6. As stated by Kiratzi *et al.* (2003), the Strofades earthquake is characterized by source complexity. Because STRF shows a much larger displacement than KERI—although the latter is closer to the main source—we suppose that the large displacement was caused by a strong aftershock (M5.5; 6 min after the main shock) close to the island of Strofades (see Fig. 6). Given the co-seismic displacements detected, a linear fit over the whole time span is not an adequate model to describe the motion of these sites. The time-series suggest

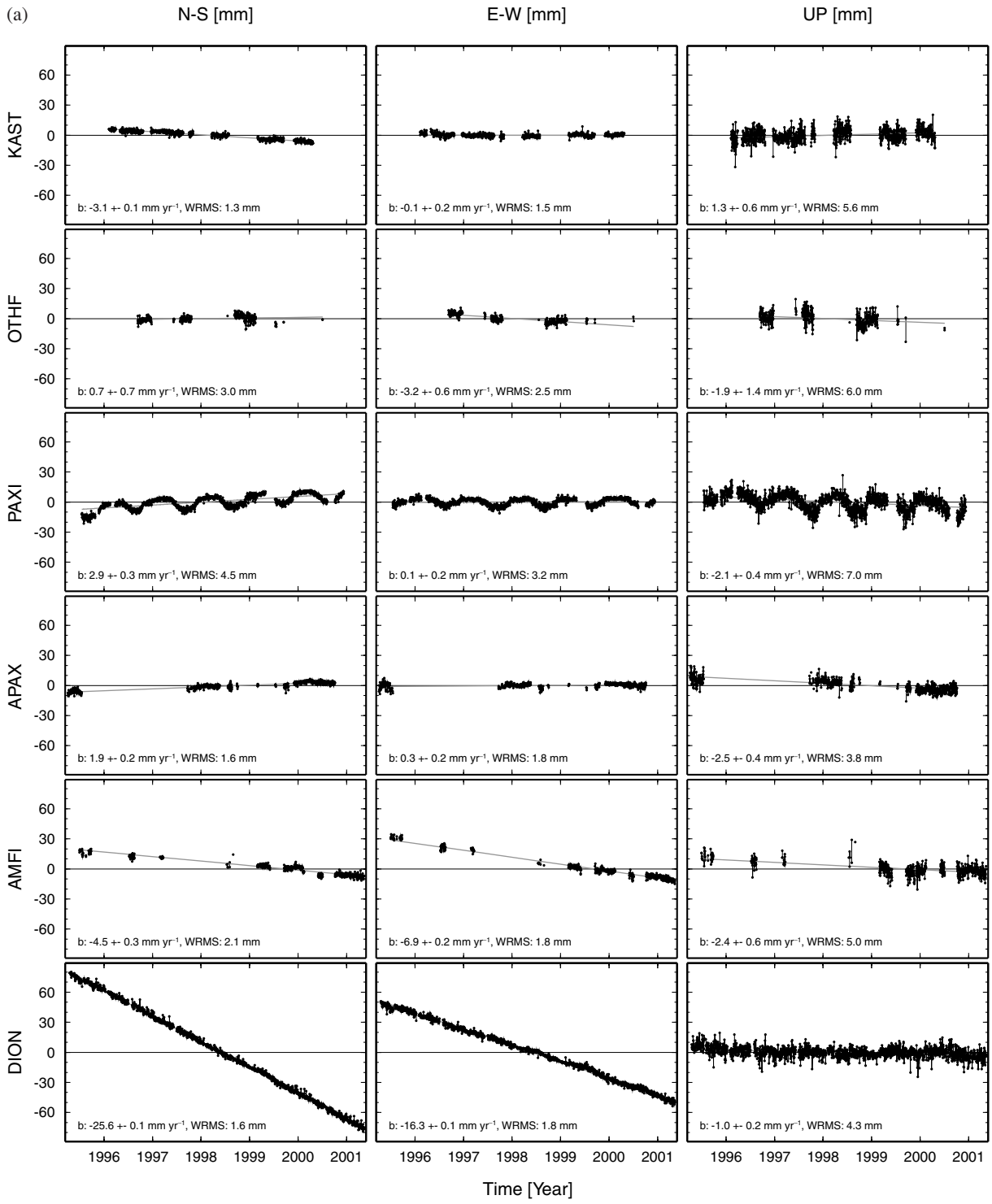

Figure 5. Common-mode filtered time-series of daily coordinates relative to Eurasia. 'b': velocity, calculated by weighted linear regression, formal error scaled by 4 (see chapter 4); b1: before, b2 after the Strofades earthquake. 'WRMS': weighted rms of daily coordinates. The grey lines represent the weighted linear fit.

that before and after the earthquake, the rates can be described as linear. The velocities before and after the event are even identical within the margin of error. In this context, it is pointed out that the improvement of the time-series is of utmost importance. It is evident for the site KERI: before the improvement, linear regressions for the east component yielded different velocities for the time spans before and after the earthquake (2.8 mm yr^{-1}). With each step of improvement, the pre- and post-seismic velocities became more and more similar (Fig. 3). At the end, they were equal within the noise level given. The velocity of crustal motion resumed the previous rate after the earthquake. Without the improvement of the time-series, a false interpretation would have been made.

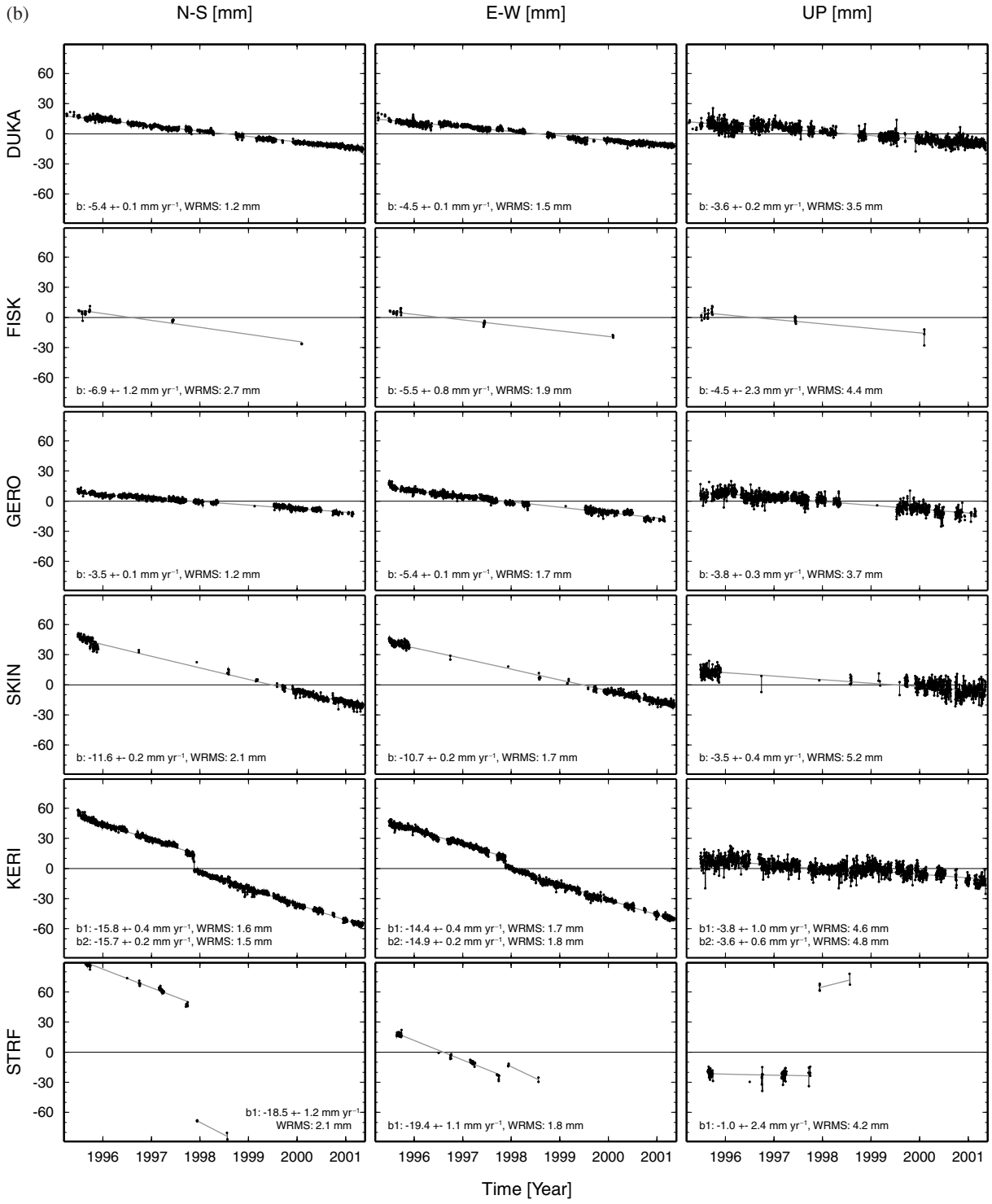

Figure 5. (*Continued.*)

The trajectory of DION shows a slight variation in the months prior to the $Mw6.0$ Athens earthquake on 1999 September 7. However, the interpretation in connection with the fault plane solution is not possible in this case.

The filtered time-series allowed—for the first time—to obtain reliable results of vertical motion in the Ionian region. The relatively high uncertainties of GPS-heights, including systematic error sources (such as setup errors and unknown antenna phase centre variations), made it impossible to arrive at reliable results with a postulated significance when only campaign measurements were used. Even with continuous measurements, but without time-series improvement, it is difficult to obtain reliable height results—as the example of KERI proves (Fig. 3). Also the filtered time-series must have a certain length (>4 yr) and completeness in order to provide significant results at an accuracy level of less than 2 mm yr^{-1}. The finally obtained vertical rates are displayed in Fig. 6, inset b)

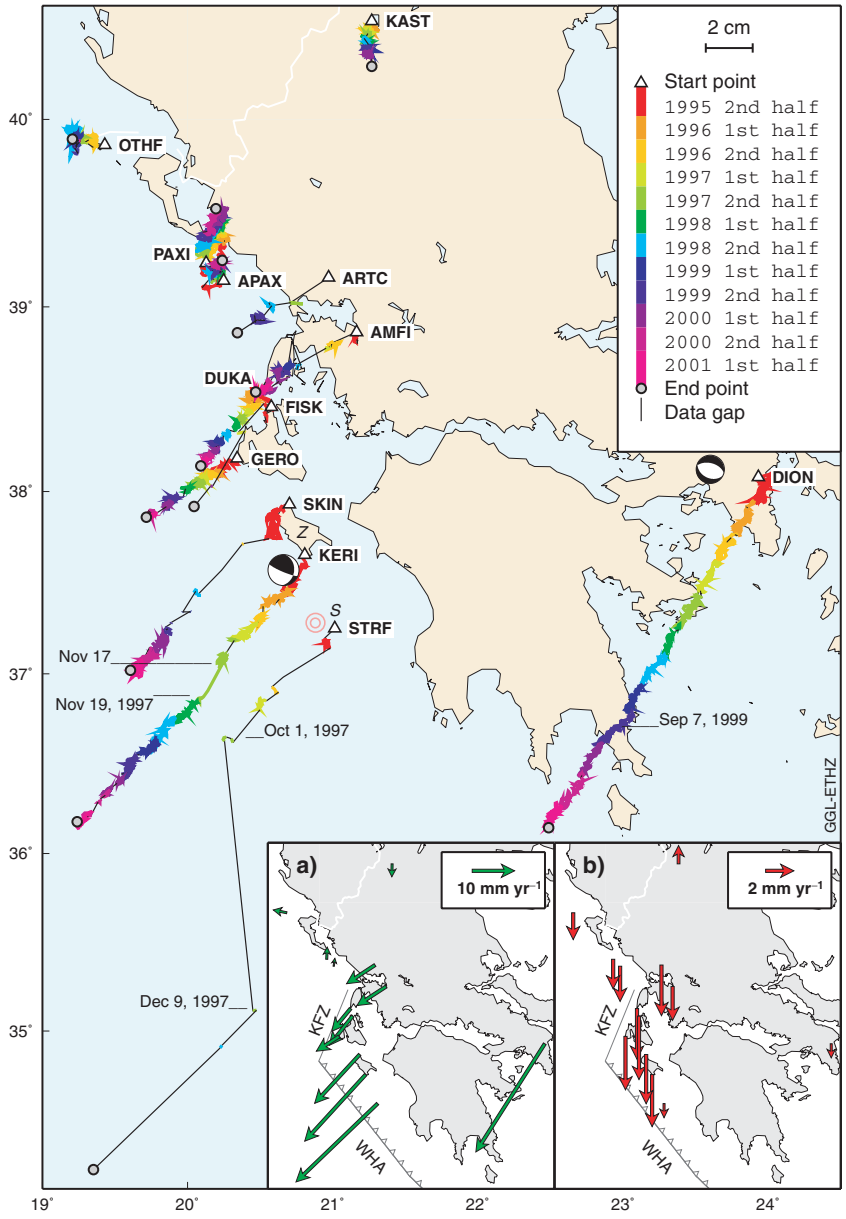

Figure 6. GPS-trajectories of horizontal crustal motion 1995–2001 relative to Eurasia, produced from common-mode filtered daily coordinate time-series, smoothed with a Gaussian filter (window: 7 days). The start points of the trajectories are at the same time the locations of the sites. The fault plane solutions (fps) represent the large earthquakes which occurred on 1997 November 18 near STRF and on 1999 September 7 near DION, while the red circles mark the strong aftershocks 6 min after the Strofades earthquake (fps: Harvard CMT solutions, http://www.seismology.harvard.edu; locations: USGS-NEIC, http://gldss7.cr.usgs.gov/neis/epic/epic.html). Insets: Horizontal (a) and vertical (b) GPS-velocities calculated by weighted linear regression of common-mode filtered coordinate time-series (numerical values and errors see Table 1). For KERI and STRF, velocity 1 (before the Strofades earthquake) is plotted. KFZ: Kephalonia Fault Zone, WHA: West Hellenic Arc, S: Strofades, Z: Zakinthos.

(compare also Table 1). Northern Greece (KAST) shows a rate of about 1 mm yr^{-1}. In the northern Ionian sea region (to the north of the KFZ), the vertical velocities are around −2 to −2.5 mm yr^{-1}, and in the southern Ionian sea around −3.5 to −4.5 mm yr^{-1}. In comparison, the vertical rates of the 19 Eurasian stations (used for the calculation of the Euler pole) are on average −0.5 mm yr^{-1}. This means that the WHA area is currently characterized by interseismic subsidence, which is in contrast to the geologically evident long-term uplift. A possible conclusion is that the uplift is caused by co-seismic effects. This is confirmed by the Strofades earthquake. Another example is the pronounced co-seismic uplift of Kephalonia caused by the *Ms*7.2 Kephalonia earthquake in 1953 (Stiros *et al.* 1994). In the time period between the earthquakes, the Hellenic side of the arc is pulled down by the subducted African plate until the stress becomes too large and is released during a seismic event.

One of the central scientific questions in the bordering vicinity of the WHA relates to the southeastern boundary of the so-called Adriatic microplate. Based on previous analyses of GPS data (see e.g. Hollenstein *et al.* 2003; Serpelloni *et al.* 2005), it has become possible to identify a northeast oriented motion of Apulia (e.g. Matera or Specchia Christi) of 4 mm yr^{-1} in a Eurasia-fixed frame. Due to the geographically limited extent of our CGPS network in Greece, it cannot be identified where the boundary of the Adriatic plate is exactly located. However, judging from the rates of

Table 1. GPS-velocities relative to Eurasia calculated by weighted linear regression of common-mode filtered coordinate time-series (1995–2001).

Site	Lon (°)	Lat (°)	v_n (mm yr^{-1})	v_e (mm yr^{-1})	v_u (mm yr^{-1})	σ_{v_n} (mm yr^{-1})	σ_{v_e} (mm yr^{-1})	σ_{v_u} (mm yr^{-1})	WRMS$_n$ (mm)	WRMS$_e$ (mm)	WRMS$_u$ (mm)
KAST	21.2686	40.5193	−3.1	−0.1	1.3	0.1	0.2	0.6	1.3	1.5	5.6
OTHF	19.4292	39.8649	0.7	−3.2	−1.9	0.7	0.6	1.4	3.0	2.5	6.0
PAXI	20.1282	39.2356	2.9	0.1	−2.1	0.3	0.2	0.4	4.5	3.2	7.0
APAX	20.2486	39.1406	1.9	0.3	−2.5	0.2	0.2	0.4	1.6	1.8	3.8
ARTC	20.9713	39.1572	−4.4	−6.7	−3.6	1.3	1.8	3.8	1.9	2.8	5.7
AMFI	21.1648	38.8641	−4.5	−6.9	−2.4	0.3	0.2	0.6	2.1	1.8	5.0
DION	23.9326	38.0785	−25.6	−16.3	−1.0	0.1	0.1	0.2	1.6	1.8	4.3
DUKA	20.5425	38.5635	−5.4	−4.4	−3.6	0.1	0.1	0.2	1.2	1.5	3.5
FISK	20.5773	38.4599	−6.9	−5.5	−4.5	1.2	0.8	2.3	2.7	1.9	4.4
GERO	20.3416	38.1802	−3.5	−5.4	−3.8	0.1	0.1	0.3	1.2	1.7	3.7
SKIN	20.7022	37.9309	−11.6	−10.7	−3.5	0.2	0.2	0.4	2.1	1.7	5.2
KERI	20.8081	37.6547	−20.0	−17.4	−3.2	0.3	0.2	0.3	5.0	3.4	4.7
KERI1	20.8081	37.6547	−15.8	−14.4	−3.8	0.4	0.4	1.0	1.6	1.7	4.6
KERI2	20.8081	37.6547	−15.7	−14.9	−3.6	0.2	0.2	0.6	1.5	1.8	4.8
STRF	21.0142	37.2500	−37.2	−17.4	9.7	14.8	1.8	10.1	28.2	3.5	19.2
STRF1	21.0142	37.2500	−18.5	−19.4	−1.0	1.2	1.1	2.4	2.1	1.8	4.2

n: north-component, e: east-component, u: up-component; v: velocity; σ_v: formal velocity error scaled by 4 (see chapter 4); WRMS: weighted rms of daily coordinates. 1/2 appended to the site name: only data before/after the Strofades earthquake are used for the linear regression.

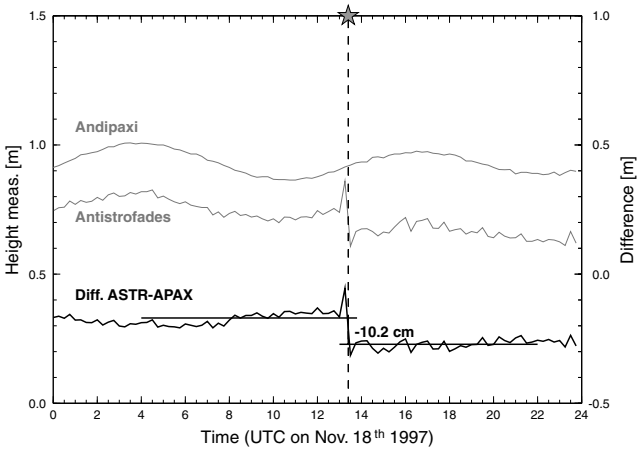

Figure 7. Tide gauge measurements on the islands of Andipaxi (near APAX) and Antistrofades (near STRF) for the day of the Strofades earthquake. The tide gauge measurement at Andipaxi (not affected by the earthquake) was used as reference in order to remove the tides from the see level at Antistrofades (ASTR). The difference reveals an apparent co-seismic change of the mean sea level (10.2 cm) in Antistrofades which was caused by the uplift of the island. The star and the dashed line indicate the time of the earthquake.

the stations OTHF, PAXI and APAX, it is evident that these northern Ionian islands are occupied by a kinematic pattern that is characterized by a clearly north/northwest oriented motion relative to Eurasia. As such these sites move completely different from the Anatolian–Aegean microplate, but they are also not similar to the Adriatic motion pattern. The southeastern boundary of the Adriatic microplate will, therefore, have to be sought to the north–northwest of the Ionian islands.

6 CONCLUSIONS

From GPS time-series, a crustal deformation history of high temporal resolution was determined. In seismically active regions like Greece, it cannot a priori be assumed that the movements are linear, especially when local earthquakes cause displacements. Therefore, it is of advantage to study time-series to shed light on the temporal behaviour of the motions. Trajectories are a good representation to visualize also the spatial distribution of crustal deformation.

To ensure a consistent Eurasia-fixed reference frame, we included 54 IGS/EUREF sites in the evaluation, constrained the network by Helmert transformation to a subset of 15 IGS sites and estimated a consistent pole of rotation for Eurasia.

With the strategy of improving the time-series, systematic errors can be reduced, and the precision of velocities as well as the coordinate scatter can be improved significantly. We reached an average improvement of about 40 per cent; 25 per cent relative improvement by excluding poor data (poor data of one GPS station can have a big influence on the solution of the whole network), 5 per cent by removing remaining outliers and 20 per cent by applying a weighted common-mode filter. The average WRMS could be reduced from 4 to 2 mm for horizontal and from 12 to 6 mm for vertical daily coordinates. Only on the basis of high-quality improved time-series, it was also possible to obtain reliable vertical velocities.

For the WHA area, we could confirm and refine the following results of Cocard *et al.* (1999): increasing horizontal rates from north to south, dextral shear strain in the KFZ, large baseline lengthening on the island of Zakinthos and co-seismic horizontal displacements of up to 12 cm caused by the $Mw6.6$ Strofades earthquake in 1997.

In addition, we were able to show that there is a significant southward motion in northern Greece and adjacent regions to the north. While the seismic activity in the WHA area is relatively high, the motion of most of the sites is surprisingly linear during the 6 yr analysed. The most striking deviations from linearity are the co-seismic slips caused by the Strofades earthquake. It is clearly seen that the island of Strofades was uplifted by about 9 cm and that there is no significant difference between the velocities before and after the earthquake. The trajectory of the site DION near Athens shows a slight variation in the months prior to the 1999 Athens $Mw6.0$ earthquake. Another very interesting result is the fact that the Ionian islands are characterized by interseismic subsidence of up to 4 mm yr^{-1}.

ACKNOWLEDGMENTS

The contribution of Stelios Felekis during all stages of field work is gratefully acknowledged. We are grateful to the Directors of the Lighthouse Authority of the Hellenic Navy, the Director of the Byzantine Museum of the city of Kastoria, the prefect of the city of Amfilochia, Gelli Koyiadi of the city of Arta, and the director of the Natural and Environmental Museum of the city of Fiskardo, who helped us by providing site-hosting facilities for the GPS stations. We thank Profs Billiris and Paradissis of the NTU Athens for their continued support, and Dani Galanis for providing continuous GPS data of the station DION. We are grateful to Prof M. Cocard, Université Laval, Canada, for thoughtful comments and help at an earlier stage of this project. Valuable comments of the editor and the reviewers substantially helped to improve the manuscript. Funds were provided by ETH grant No. 41-2647.5 and EU grant No. ENV4-CT97-0519 provided by the Swiss Federal Office of Education and Science.

REFERENCES

Altamimi, Z., Sillard, P. & Boucher, C., 2002. ITRF2000: a new release of the International Terrestrial Reference Frame for earth science applications, *J. geophys. Res.,* **107**(B10), 2214, doi:10.1029/2001JB000561.

Beutler, G. *et al.*, 2001. *Bernese GPS Software Version 4.2*, eds Hugentobler, U., Schaer, S. & Fridez, P., Astronomical Institute, University of Berne, Switzerland.

Caporali, A., 2003. Average strain rate in the Italian crust inferred from a permanent GPS network—I. Statistical analysis of the time-series of permanent GPS stations, *Geophys. J. Int.,* **155,** 241–253.

Cocard, M., Kahle, H.-G., Peter, Y., Geiger, A., Veis, G., Felekis, S., Billiris, H. & Paradissis, D., 1999. New constraints on the rapid crustal motion of the Aegean region: recent results inferred from GPS measurements (1993–1998) across the West Hellenic Arc, Greece, *Earth planet. Sci. Lett.,* **172,** 39–47.

Heller, O., 2004. *GPS-Zeitreihenanalyse zur Bestimmung tektonischer Bewegungen*, *Diploma thesis*, Institute of Geodesy and Photogrammetry, ETH Zürich.

Hollenstein, Ch., 2000. *Zeitreihenanalyse kontinuierlicher GPS-Messungen zur Bestimmung tektonischer Bewegungen im Gebiet der Ionischen Inseln*, Diploma thesis, Institute of Geodesy and Photogrammetry, ETH Zürich.

Hollenstein, Ch., Kahle, H.-G., Geiger, A., Jenny, S., Goes, S. & Giardini, D., 2003. New GPS constraints on the Africa-Eurasia plate boundary zone in southern Italy, *Geophys. Res. Lett.,* **30**(18), 1935, doi:10.1029/2003GL017554.

Kahle, H.-G., Müller, M.V., Geiger, A., Danuser, G., Müller, S., Veis, G., Billiris, H. & Paradissis, D., 1995. The strain field in NW Greece and the Ionian Islands: results inferred from GPS measurements, *Technophysics,* **249,** 41–52.

Kiratzi, A. & Louvari, E., 2003. Focal mechanisms of shallow earthquakes in the Aegean Sea and the surrounding lands determined by waveform modelling: a new database, *J. Geodyn.,* **36,** 251–274.

Kouba, J., 2002. The GPS toolbox ITRF transformations, *GPS Solutions,* **5**(3), 88–90.

Laigle, M., Sachpazi, M. & Hirn, A., 2004. Variation of seismic coupling with slab detachment and upper plate structure along the western Hellenic subduction zone, *Technophys.,* **391,** 85–95.

Mao, A., Harrison, C.G.A. & Dixon, T.H., 1999. Noise in GPS coordinate time series, *J. geophys. Res.,* **104**(B2), 2797–2816.

Niell, A., 1996. Global mapping functions for the atmosphere delay at radio wavelengths, *J. geophys. Res.,* **101**(B2), 3227–3246.

Peter, Y., 2001. Present-day crustal dynamics in the Adriatic-Aegean plate boundary zone inferred from continuous GPS-measurements, *PhD thesis*, Mitteilungen Nr. 71, Institute of Geodesy and Photogrammetry, ETH Zürich.

Peter, Y., Kahle, H.-G., Cocard, M., Veis, G., Felekis, S. & Paradissis, D., 1998. Establishment of a continuous GPS network across the Kephalonia Fault Zone, Ionian Islands, Greece, *Technophys.,* **294,** 253–260.

Serpelloni, E., Anzidei, M., Baldi, P., Casula, G. & Galvani, A., 2005, Crustal velocity and strain-rate fields in Italy and surrounding regions: new results from the analysis of permanent and non-permanent GPS networks, *Geophys. J. Int.,* **161,** 861–880, doi:10.1111/j.1365-246X.2005.02618.x.

Stiros, S.C., Pirazzoli, P.A., Laborel, J. & Laborel-Deguen, F., 1994. The 1953 earthquake in Cephalonia (Western Hellenic Arc): coastal uplift and halotectonic faulting, *Geophys. J. Int.,* **117**(3), 834–849.

Wdowinski, S., Bock, Y., Zhang, J., Fang, P. & Genrich, J., 1997. Southern California Permanent GPS Geodetic Array: spatial filtering of daily position for estimating coseismic and postseismic displacements induced by the 1992 Landers earthquake, *J. geophys. Res.,* **102**(B8), 18 057–18 070.

Zhang, J., Bock, Y., Johnson, H., Fang, P., Williams, S., Genrich, J., Wdowinski, S. & Behr, J., 1997. Southern California Permanent GPS Geodetic Array: error analysis of daily position estimates and site velocities, *J. geophys. Res.,* **102**(B8), 18 035–18 055.